

# SOLVING THE $S_N$ NEUTRON TRANSPORT EQUATION USING HIGH ORDER LAX–FRIEDRICHS WENO FAST SWEEPING METHODS

Dean Wang<sup>1\*</sup>, Tseelmaa Byambaakhuu<sup>1</sup>, Sebastian Schunert<sup>2</sup>, Zeyun Wu<sup>3</sup>

<sup>1</sup>Department of Mechanical and Aerospace Engineering  
The Ohio State University  
201 W 19th Avenue, Columbus, OH 43210, USA

<sup>2</sup>Nuclear Engineering Methods Development  
Idaho National Laboratory, Idaho Falls, ID, USA

<sup>3</sup>Department of Mechanical and Nuclear Engineering  
Virginia Commonwealth University  
800 E. Leigh St., Richmond, VA 23219, USA

wang.12239@osu.edu, byambaakhuu.1@osu.edu, sebastian.schunert@inl.gov, zwu@vcu.edu

## ABSTRACT

Recently we have proposed high order Lax–Friedrichs WENO (LF-WENO) fast sweeping methods for solving the  $S_N$  neutron transport equation and demonstrated their superior performance in terms of accuracy, convergence, and positivity preserving property [1]. It was found in our previous work that LF-WENO3 can achieve better spatial convergence rate than the diamond difference (DD) method; however both methods do not attain their theoretical order of accuracy in spatial discretization because of lack of sufficient smoothness in the solution of the model problem tested. In the present paper, we further investigate the spatial convergence performance of LF-WENO3 for the  $S_N$  solution based on the manufactured solutions. Numerical results are presented that show the expected third-order spatial convergence rate of LF-WENO3. In addition, we present in detail numerical analysis of the performance of LF-WENO3 for thick diffusive problems in comparison with the DD and step characteristic (SC) schemes.

KEYWORDS:  $S_N$ , LF-WENO, diffusion limit

## 1. INTRODUCTION

Fast sweeping methods are efficient iterative techniques originally developed to solve the steady state Hamilton-Jacobi equations and successfully applied for the hyperbolic conservation laws recently [2]. These fast sweeping methods achieve very fast convergence based on a Gauss–Seidel type nonlinear

---

\* Corresponding author

iteration approach and the alternating direction sweeping by taking advantage of the transport information propagation property. The LF-WENO fast sweeping method was originally developed by Chen et al. [3].

Recently we proposed the LF-WENO fast sweeping methods for solving the  $S_N$  neutron transport equation and demonstrated their superior performance in terms of accuracy, convergence, and positivity preserving property [1]. In this paper, we extend our previous study of LF-WENO3 by comparing numerical results against manufactured solutions which possess arbitrary smoothness. It is well known that diffusion theory is an asymptotic limit of transport theory for physical systems in which the total cross section  $\Sigma_t$  is large and the absorption cross section  $\Sigma_a$  and source  $Q$  are small [4-8]. However, a numerical scheme for the  $S_N$  transport equation does not necessarily possess the diffusion limit. Theoretical and numerical studies of various discretization schemes for the  $S_N$  equation can be found in [9-13]. In this paper, we study the performance of LF-WENO3 for thick diffusive problems.

## 2. HIGH ORDER LAX–FRIEDRICHS WENO FAST SWEEPING METHODS

### 2.1. Two-Dimensional $S_N$ Neutron Transport Equation

Note the details of the LF-WENO3 method for the  $S_N$  transport equation have been published elsewhere [1]. For completeness, we recast them as follows. We consider the monoenergetic neutron transport fixed-source problems on 2-D Cartesian geometry.

$$\mu \frac{\partial}{\partial x} \psi(x, y, \mu, \eta) + \eta \frac{\partial}{\partial y} \psi(x, y, \mu, \eta) + \Sigma_t \psi(x, y, \mu, \eta) = \frac{\Sigma_s}{4} \phi(x, y) + \frac{1}{4} Q(x, y), \quad (1a)$$

where  $\phi$  and  $\psi$  are the scalar flux and angular flux, respectively, and

$$\phi(x, y) = \int \psi(x, y, \mu, \eta) d\mu d\eta, \quad (1b)$$

$\Sigma_t$  and  $\Sigma_s$  are the total cross section and scattering cross section,  $\mu$  and  $\eta$  are the neutron angular directions.  $x$  and  $y$  are the spatial positions, and  $Q$  is the external neutron source. We assume isotropic scattering and neutron source.

To simplify notation, we write Eq. (1a) in the conservative form as

$$f(\psi)_x + g(\psi)_y + \Sigma_t \psi = s(\psi, x, y), \quad (x, y) \in [0, a] \times [0, b], \quad (2)$$

where,

$$f(\psi) = \mu \psi, \quad (3a)$$

$$g(\psi) = \eta \psi, \quad (3b)$$

$$s(\psi, x, y) = \frac{\Sigma_s}{4} \phi(x, y) + \frac{1}{4} Q(x, y). \quad (3c)$$

Since the  $S_N$  equation is the constant coefficient partial differential equation, the “flux” functions,  $f(\psi)$  and  $g(\psi)$ , are a linear function of  $\psi$ . However, in many hyperbolic conservation equations such as flow transport equations they are nonlinear and therefore the solution could develop singularities or shocks.

Let  $\{(x_i, y_j)\}$ ,  $i = 1, \dots, N_x$ ,  $j = 1, \dots, N_y$  denote the cell center points of a uniform discretization of the computational domain, with  $\Delta x = a/N_x$  and  $\Delta y = b/N_y$  as the mesh sizes for  $x$  and  $y$  direction,

respectively. We use  $\psi_{i,j}$  to represent the numerical solution of  $\psi$  in the cell  $(x_i, y_j)$ . A conservative finite difference discretization of Eq. (2) can be written as

$$\frac{\hat{f}_{i+\frac{1}{2},j} - \hat{f}_{i-\frac{1}{2},j}}{\Delta x} + \frac{\hat{g}_{i,j+\frac{1}{2}} - \hat{g}_{i,j-\frac{1}{2}}}{\Delta y} + \Sigma_t \psi_{i,j} = s(\psi_{i,j}, x_i, y_j), \quad (4)$$

in which  $\hat{f}_{i\pm\frac{1}{2},j}$  and  $\hat{g}_{i,j\pm\frac{1}{2}}$  represent numerical flux approximations at  $(x_{i\pm\frac{1}{2}}, y_j)$  and  $(x_i, y_{j\pm\frac{1}{2}})$ , respectively. Therefore, the accuracy order of the numerical method depends on the order of the numerical flux approximation of  $f(\psi)_x$  and  $g(\psi)_y$ . We will approximate them using high order Lax–Friedrichs WENO numerical fluxes. It is noted that  $\psi_{i,j}$  is actually the average value over the cell for conservative schemes.

## 2.2. Construction of High Order WENO Fluxes

To develop a higher order sweeping method, one needs high order numerical fluxes in Eq. (4). In this section, we briefly review the construction of numerical fluxes for high order finite difference WENO schemes.

The numerical flux  $\hat{f}_{i+\frac{1}{2},j}$  (or  $\hat{g}_{i,j+\frac{1}{2}}$ ) is computed through the neighboring cell values  $f_{i,j} = f(\psi_{i,j})$  along the  $x$  direction (or the  $y$  direction). For a  $(2K - 1)$ th order WENO scheme, the  $K$  numerical fluxes are computed as

$$\hat{f}_{i+\frac{1}{2},j}^{(r)} = \sum_{k=0}^{K-1} c_{rk} f_{i-r+k,j}, \quad r = 0, \dots, K - 1, \quad (5)$$

which corresponds to  $K$  different candidate stencils  $S_r(i) = \{(x_{i-r}, y_j), \dots, (x_{i-r+K-1}, y_j)\}$ ,  $r = 0, \dots, K - 1$ . Each of these numerical fluxes is  $k$ th order accurate. For example, it is the third order WENO scheme when  $K = 2$ . The two second order accurate numerical fluxes for  $\mu > 0$  are given as

$$\hat{f}_{i+\frac{1}{2},j}^{(0)} = \frac{1}{2} f_{i,j} + \frac{1}{2} f_{i+1,j}, \quad (6a)$$

$$\hat{f}_{i+\frac{1}{2},j}^{(1)} = -\frac{1}{2} f_{i-1,j} + \frac{3}{2} f_{i,j}. \quad (6b)$$

The  $(2K - 1)$ th order WENO flux is a superposition of all these  $K$  numerical fluxes

$$\hat{f}_{i+\frac{1}{2},j} = \sum_{k=0}^{K-1} w_k \hat{f}_{i+\frac{1}{2},j}^{(k)}. \quad (7)$$

The nonlinear weights  $w_k$  satisfy  $w_k \geq 0$ ,  $\sum_{k=0}^{K-1} w_k = 1$ , and are defined in the following way

$$w_k = \frac{\alpha_k}{\sum_{k=0}^{K-1} \alpha_k}, \quad \alpha_k = \frac{d_k}{(\epsilon + \beta_k)}. \quad (8)$$

Here  $d_k$  are the linear weights which yield the  $(2K - 1)$ th order accuracy,  $\beta_k$  are the so-called ‘‘smoothness indicators’’ of the stencils  $S_r(i)$ , which measure the smoothness of the function  $f(\psi)$ . The constant  $\epsilon$  is a small positive number used to avoid the denominator to become zero and is typically taken as  $10^{-6}$ .

For the third order WENO scheme ( $K = 2$ ), the linear weights are given by

$$d_0 = \frac{2}{3}, \quad d_1 = \frac{1}{3}, \quad (9)$$

and the smoothness indicators are given by

$$\beta_0 = \tau_0 (f_{i+1,j} - f_{i,j})^2, \beta_1 = \tau_1 (f_{i,j} - f_{i-1,j})^2, \quad (10)$$

where

$$\tau_0 = a * \max \left[ \text{abs} \left( \Sigma_{t_{i+1,j}} - \Sigma_{t_{i,j}} \right), \text{abs} \left( \Sigma_{s_{i+1,j}} - \Sigma_{s_{i,j}} \right) \right] \Delta x, \quad (11a)$$

$$\tau_1 = b * \max \left[ \text{abs} \left( \Sigma_{t_{i,j}} - \Sigma_{t_{i-1,j}} \right), \text{abs} \left( \Sigma_{s_{i,j}} - \Sigma_{s_{i-1,j}} \right) \right] \Delta x. \quad (11b)$$

Note that the WENO3 method essentially becomes the third order upwind scheme when  $\beta_0 = \beta_1 = 0$ . Here we introduce two additional parameters,  $\tau_0$  and  $\tau_1$ , to define local material (i.e., cross section) heterogeneity, which are multiplied with the original smoothness indicators. They are the differences of local neutron total cross sections or scattering cross section between the adjacent computational cells. The purpose is to recover the third order accuracy of WENO3 for smooth regions where  $\tau_0 = \tau_1 = 0$ . The coefficients  $a$  and  $b$  are used to control the magnitude of the differences of cross sections to obtain the optimal accuracy, which can be determined based on numerical experiments. When  $\mu < 0$  the right biased stencil with numerical values  $f_{i,j}$ ,  $f_{i+1,j}$  and  $f_{i+2,j}$  are used to construct a third order WENO approximation to the numerical flux  $\hat{f}_{i+\frac{1}{2},j}$ . Similar procedures are used for the  $y$  direction  $g(\psi)_y$ .

### 2.3. Lax-Friedrichs Sweeping Framework

As proposed in [3], here we use Lax-Friedrichs WENO fluxes to obtain the high order sweeping method. First, we define

$$\hat{f}_{i+\frac{1}{2},j} = \hat{f}_{i+\frac{1}{2},j} + \frac{\sigma\mu}{2} (\psi_{i+1,j} - \psi_{i,j}), \quad i = 1, \dots, N_x, \quad (12a)$$

$$\hat{g}_{i,j+\frac{1}{2}} = \hat{g}_{i,j+\frac{1}{2}} + \frac{\sigma\eta}{2} (\psi_{i,j+1} - \psi_{i,j}), \quad j = 1, \dots, N_y, \quad (12b)$$

where  $\hat{f}_{i+\frac{1}{2},j}$  and  $\hat{g}_{i,j+\frac{1}{2}}$  are the high order WENO flux in the  $x$  and  $y$  directions, respectively. The relaxation factor,  $\sigma$ , can be adjusted to improve the convergence rate. It is found that a number less than 1.0 can speed up the convergence. However, the scheme would become unstable and fail to converge if it is too small. Then we have

$$\hat{f}_{i+\frac{1}{2},j} = \hat{f}_{i+\frac{1}{2},j} - \frac{\sigma\mu}{2} (\psi_{i+1,j} - \psi_{i,j}), \quad i = 1, \dots, N_x, \quad (13a)$$

$$\hat{g}_{i,j+\frac{1}{2}} = \hat{g}_{i,j+\frac{1}{2}} - \frac{\sigma\eta}{2} (\psi_{i,j+1} - \psi_{i,j}), \quad j = 1, \dots, N_y. \quad (13b)$$

The above formulae mimic the first order Lax-Friedrichs formulation, which allows us to develop the iterative scheme. The discretization formula Eq. (4) then can be rewritten, in terms of  $\hat{f}_{i+\frac{1}{2},j}$  and  $\hat{g}_{i,j+\frac{1}{2}}$ , as

$$\frac{\hat{f}_{i+\frac{1}{2},j} - \frac{\sigma\mu}{2}(\psi_{i+1,j} - \psi_{i,j}) - \hat{f}_{i-\frac{1}{2},j} + \frac{\sigma\mu}{2}(\psi_{i,j} - \psi_{i-1,j})}{\Delta x} + \frac{\hat{g}_{i,j+\frac{1}{2}} - \frac{\sigma\eta}{2}(\psi_{i,j+1} - \psi_{i,j}) - \hat{g}_{i,j-\frac{1}{2}} + \frac{\sigma\eta}{2}(\psi_{i,j} - \psi_{i,j-1})}{\Delta y} + \Sigma_t \psi_{i,j} = s(\psi_{i,j}, x_i, y_j). \quad (14)$$

We have

$$\begin{aligned} \psi_{i,j} &= \frac{s(\psi_{i,j}, x_i, y_j) \Delta x \Delta y - \left[ \hat{f}_{i+\frac{1}{2},j} - \hat{f}_{i-\frac{1}{2},j} - \frac{\sigma\mu}{2}(\psi_{i+1,j} + \psi_{i-1,j}) \right] \Delta y - \left[ \hat{g}_{i,j+\frac{1}{2}} - \hat{g}_{i,j-\frac{1}{2}} - \frac{\sigma\eta}{2}(\psi_{i,j+1} + \psi_{i,j-1}) \right] \Delta x}{\sigma(\mu\Delta y + \eta\Delta x) + \Sigma_t \Delta x \Delta y} \\ &= \frac{s(\psi_{i,j}, x_i, y_j) \Delta x - \left[ \hat{f}_{i+\frac{1}{2},j} - \hat{f}_{i-\frac{1}{2},j} - \frac{\sigma\mu}{2}(\psi_{i+1,j} + \psi_{i-1,j}) \right] - \left[ \hat{g}_{i,j+\frac{1}{2}} - \hat{g}_{i,j-\frac{1}{2}} - \frac{\sigma\eta}{2}(\psi_{i,j+1} + \psi_{i,j-1}) \right] \left( \frac{\Delta x}{\Delta y} \right)}{\sigma \left[ \mu + \eta \left( \frac{\Delta x}{\Delta y} \right) \right] + \Sigma_t \Delta x} \end{aligned} \quad (15)$$

We sweep the whole domain with the following four alternating orderings repeatedly. However, they can be solved in any order since the orderings are independent.

- |      |              |             |                              |
|------|--------------|-------------|------------------------------|
| I.   | $i = 1:N_x,$ | $j = 1:N_y$ | for $\mu > 0$ and $\eta > 0$ |
| II.  | $i = N_x:1,$ | $j = 1:N_y$ | for $\mu < 0$ and $\eta > 0$ |
| III. | $i = 1:N_x,$ | $j = N_y:1$ | for $\mu > 0$ and $\eta < 0$ |
| IV.  | $i = N_x:1,$ | $j = N_y:1$ | for $\mu < 0$ and $\eta < 0$ |

If the first sweeping direction is chosen, then  $\psi_{i-1,j} = \psi_{i-1,j}^{n+1}$ ,  $\psi_{i,j-1} = \psi_{i,j-1}^{n+1}$ ,  $\psi_{i+1,j} = \psi_{i+1,j}^n$ , and  $\psi_{i,j+1} = \psi_{i,j+1}^n$ . Thus, we obtain the Gauss-Seidel iterative scheme

$$\psi_{i,j}^{n+1} = \frac{s^n(\psi_{i,j}, x_i, y_j) \Delta x - \left[ \hat{f}_{i+\frac{1}{2},j}^* - \hat{f}_{i-\frac{1}{2},j}^* - \frac{\sigma\mu}{2}(\psi_{i+1,j}^n + \psi_{i-1,j}^{n+1}) \right] - \left[ \hat{g}_{i,j+\frac{1}{2}}^* - \hat{g}_{i,j-\frac{1}{2}}^* - \frac{\sigma\eta}{2}(\psi_{i,j+1}^n + \psi_{i,j-1}^{n+1}) \right] \left( \frac{\Delta x}{\Delta y} \right)}{\sigma \left[ \mu + \eta \left( \frac{\Delta x}{\Delta y} \right) \right] + \Sigma_t \Delta x}. \quad (16)$$

Similar to the DD method, we follow the neutron characteristics and sweep through the grids with alternating directions and use the most recent flux values as we update the solution, in which  $\hat{f}^*$  and  $\hat{g}^*$  are also calculated using the newly updated flux values if available. The implementation of the LF-WENO3 method is very simple and straightforward, in particularly on a two-dimensional Cartesian mesh. Since the WENO3 stencil involves two upwind cells in each direction, the cell values near the boundary have to be carefully computed to avoid the reduction in the global accuracy. In our implementation of LF-WENO, for simplicity the DD method has been used for the boundary cells.

### 3. NUMERICAL RESULTS

#### 3.1. Spatial Discretization Convergence

In [1], we investigated the spatial convergence of the LF-WENO3 method based on a simple 1-D slab problem and a 2-D homogeneous fixed-source neutron transport problem. It was found that for the 2-D

model problem LF-WENO3 could only attain the second-order accuracy, while DD could only have the accuracy much less than second order due to lack of sufficient smoothness of the model problem.

In this paper, we use the method of manufactured solutions (MMS) to assess the convergence property of LF-WENO3. With MMS, we can have the desired order of smoothness of the solution and therefore a full convergence rate can be achieved. The spatial domain is given by the square  $[0,2] \times [0,2]$  with the dimension in cm. The manufactured solution chosen is given by:

$$\psi(x, y, \mu_k, \eta_k) = x^3 y^3 (2 - x)^3 (2 - y)^3. \quad (17)$$

This manufactured solution has several desirable properties: a) it is infinitely differentiable (and isotropic), and therefore a spatial scheme can exhibit its full convergence rate; b) it is equal to zero on the domain boundaries, and so a natural vacuum boundary condition can be used; and c) the cubic power functions in  $x$  and  $y$  decrease rapidly to zero at the domain boundary as shown in Figure 1. This helps mitigate the boundary effects on the global accuracy of the DD approximation used for the boundary cells in LF-WENO3. The source term (which is now anisotropic), can then be calculated in each direction as follows:

$$Q_k(x, y) = 4 \left[ \begin{array}{c} (24x^2 - 48x^3 + 30x^4 - 6x^5)y^3(2 - y)^3\mu_k \\ +x^3(2 - x)^3(24y^2 - 48y^3 + 30y^4 - 6y^5)\eta_k + \Sigma_t x^3 y^3 (2 - x)^3 (2 - y)^3 \\ -\Sigma_s \phi(x, y) \end{array} \right] \quad (18)$$

where

$$\phi(x, y) = \sum_{k=1}^N w_k \psi(x, y, \mu_k, \eta_k). \quad (19)$$

Since the angular flux is isotropic, we have

$$\phi(x, y) = \sum_{k=1}^N w_k \psi(x, y, \mu_k, \eta_k) = \psi(x, y, \mu_k, \eta_k) \sum_{k=1}^N w_k = 4\psi(x, y, \mu_k, \eta_k), \quad (20)$$

$$Q_k(x, y) = 4 \left[ \begin{array}{c} (24x^2 - 48x^3 + 30x^4 - 6x^5)y^3(2 - y)^3\mu_k \\ +x^3(2 - x)^3(24y^2 - 48y^3 + 30y^4 - 6y^5)\eta_k \end{array} \right] - \Sigma_a \phi(x, y). \quad (21)$$

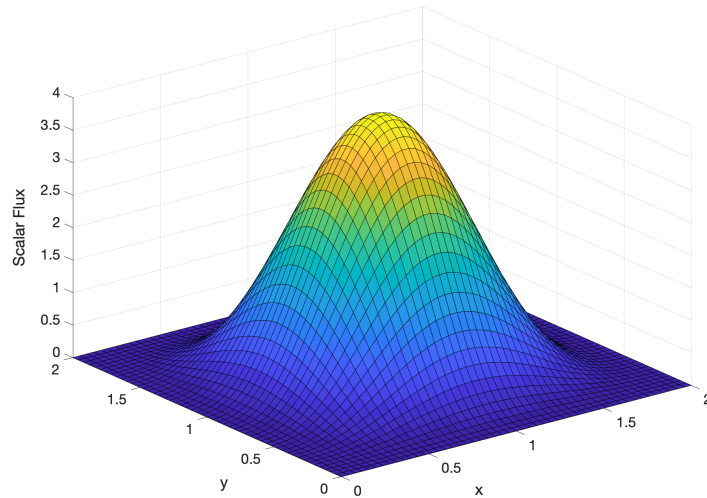


**Figure 1. Manufactured Scalar Flux.**

In this study, numerical solutions are obtained using the level-symmetric  $S_{12}$  quadrature set for angular discretization. The cell-average source for the numerical solution is obtained by averaging  $Q(x, y)$  on each computational cell. The macroscopic total cross section  $\Sigma_t = 1 \text{ cm}^{-1}$ , and the scattering cross section  $\Sigma_s = 0.6 \text{ cm}^{-1}$ . The neutron scattering source is assumed isotropic.

The flux L1 error as a function of mesh size is shown in Figure 2. With the manufactured solution, LF-WENO3 can achieve almost third-order convergence,  $\sim O(h^{2.9})$ . A slight loss of accuracy is due to the second-order DD discretization used for the boundary cells. In addition, the error is relatively large with respect to the DD results on the coarse meshes (e.g.,  $h = 0.2$  and  $0.1 \text{ cm}$ ) because the boundary cells have much larger errors than the interior ones. A higher-order approximation for the boundary cells should help improve the global accuracy of LF-WENO3. DD displays the second-order accuracy.

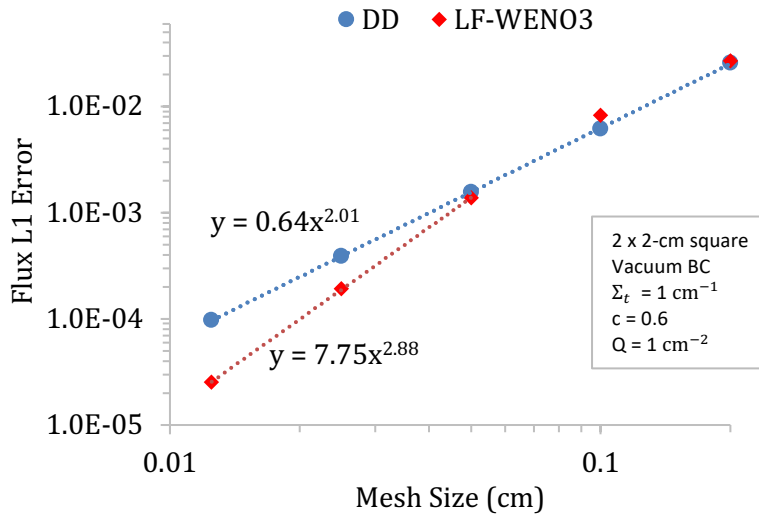


Figure 2. Flux L1 Error.

### 3.2. Thick Diffusive Problems

The above study shows that the discretization error of LF-WENO3 tends to zero as the mesh size goes to zero. This can be also verified by local truncation error analysis. Therefore, LF-WNEO3 possesses high accuracy for neutron transport problems which are typically in the optically thin regime. However, for thermal radiation transport problems, they are optically much thicker than neutron transport problems. In this section, we investigate the performance of LF-WENO3 for such thick diffusive problems based on three model problems.

The first problem is a homogeneous slab problem with the vacuum boundary on both sides. The numerical solutions are obtained using DD, SC, and LF-WENO, respectively. The Gauss–Legendre  $S_{12}$  quadrature set is used for angular discretization. The specifications of the problem are given as:

$$\begin{aligned}
 L &= 1, & h &= 0.1, \\
 \Sigma_t &= \frac{1}{\varepsilon}, & \Sigma_s &= \frac{1}{\varepsilon} - 0.8\varepsilon, \\
 Q &= \varepsilon,
 \end{aligned}$$

where  $L$  is the slab thickness and  $h$  is the mesh size in dimension of cm. The dimension of  $\Sigma_t$  and  $\Sigma_s$  is  $\text{cm}^{-1}$ . The problem becomes thick and diffusive as  $\varepsilon$  decreases, and its asymptotic solution is the same as the solution of a diffusion equation [9]:  $-\frac{d}{dx} \frac{1}{3\Sigma_t} \frac{d}{dx} \phi + \Sigma_a \phi = Q$  with  $\Sigma_t = 1\text{cm}^{-1}$ ,  $\Sigma_a = 0.8\text{cm}^{-1}$  and  $Q = 1\text{cm}^{-2}$ . Note that the diffusion length,  $\frac{1}{\sqrt{3\Sigma_t\Sigma_a}} \approx 0.65\text{cm}$ , is independent of  $\varepsilon$ . The results for various values of  $\varepsilon$  are shown in Figure 3. Note that Figure 3d depicts the scalar fluxes calculated on a finer mesh of  $h = 0.05\text{cm}$  for  $\varepsilon = 0.001$ .

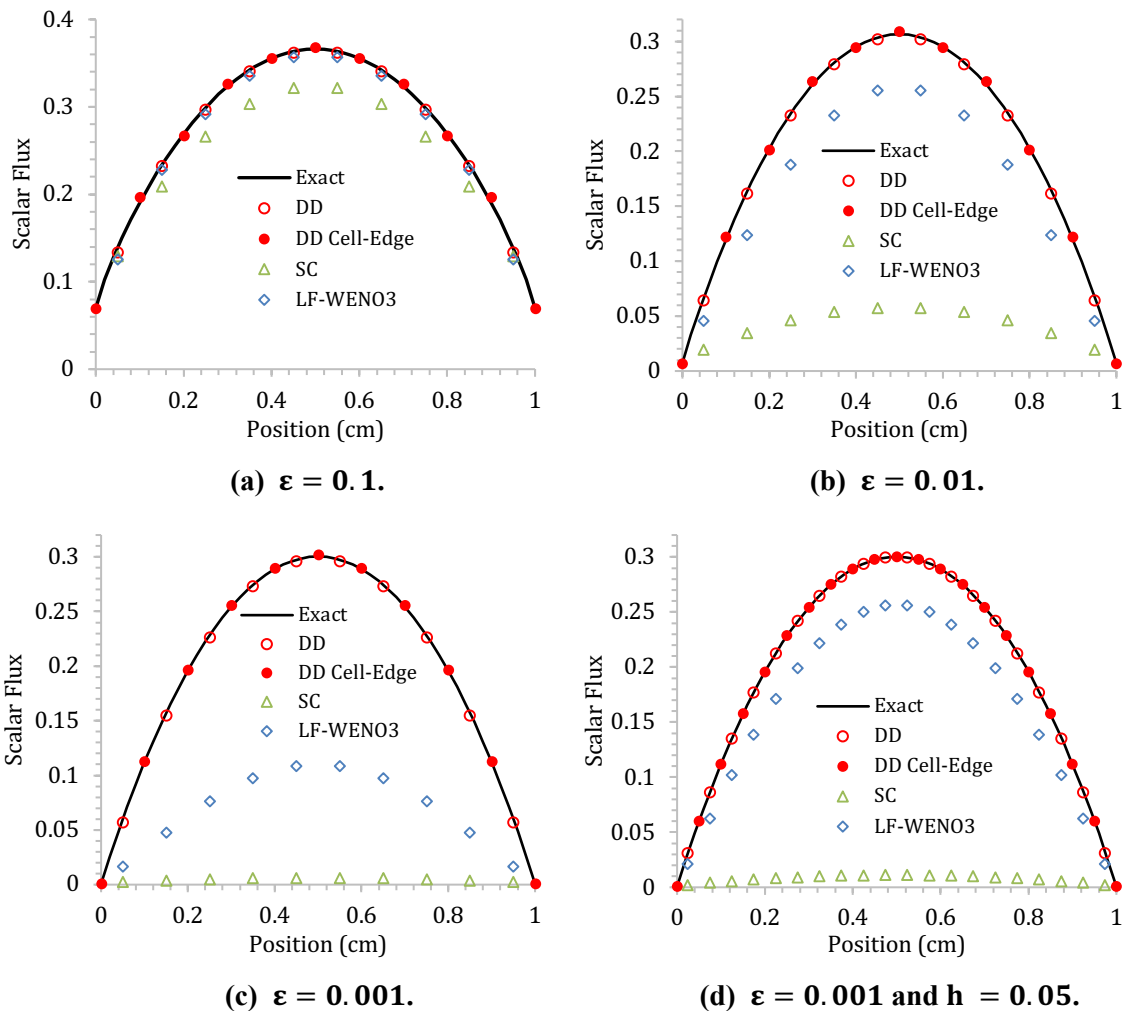


**Figure 3. 1-D Homogenous Problem.**

The second problem is an inhomogeneous slab problem with the vacuum boundary. The Gauss–Legendre  $S_{12}$  quadrature set is used for angular discretization. The problem is defined by:

$$L = 20, \quad h = 0.2,$$

$$\Sigma_t = \begin{cases} 1, & 0 < x < 5 \\ 100, & 5 < x < 10 \\ 100, & 10 < x < 20 \end{cases}, \quad \Sigma_s = \begin{cases} 0, & 0 < x < 5 \\ 90, & 5 < x < 10 \\ 99; 99.99; 99.999; 100, & 10 < x < 20 \end{cases},$$

$$Q = \begin{cases} 0, & 0 < x < 5 \\ 10, & 5 < x < 10, \\ 0, & 10 < x < 20 \end{cases}$$

The slab consists of three regions: the left region  $0 < x < 5$  is optically thin region without scattering; the middle region  $5 < x < 10$  is a thick region with the optical thickness of 20 MFPS; and the right region  $10 < x < 20$  is a thick and diffusive region where the cell optical thickness is 20 MFPS and the scattering ratio  $c$  varies from 0.99 to 1. A constant neutron source is given in the middle region. The results are shown in Figure 4.

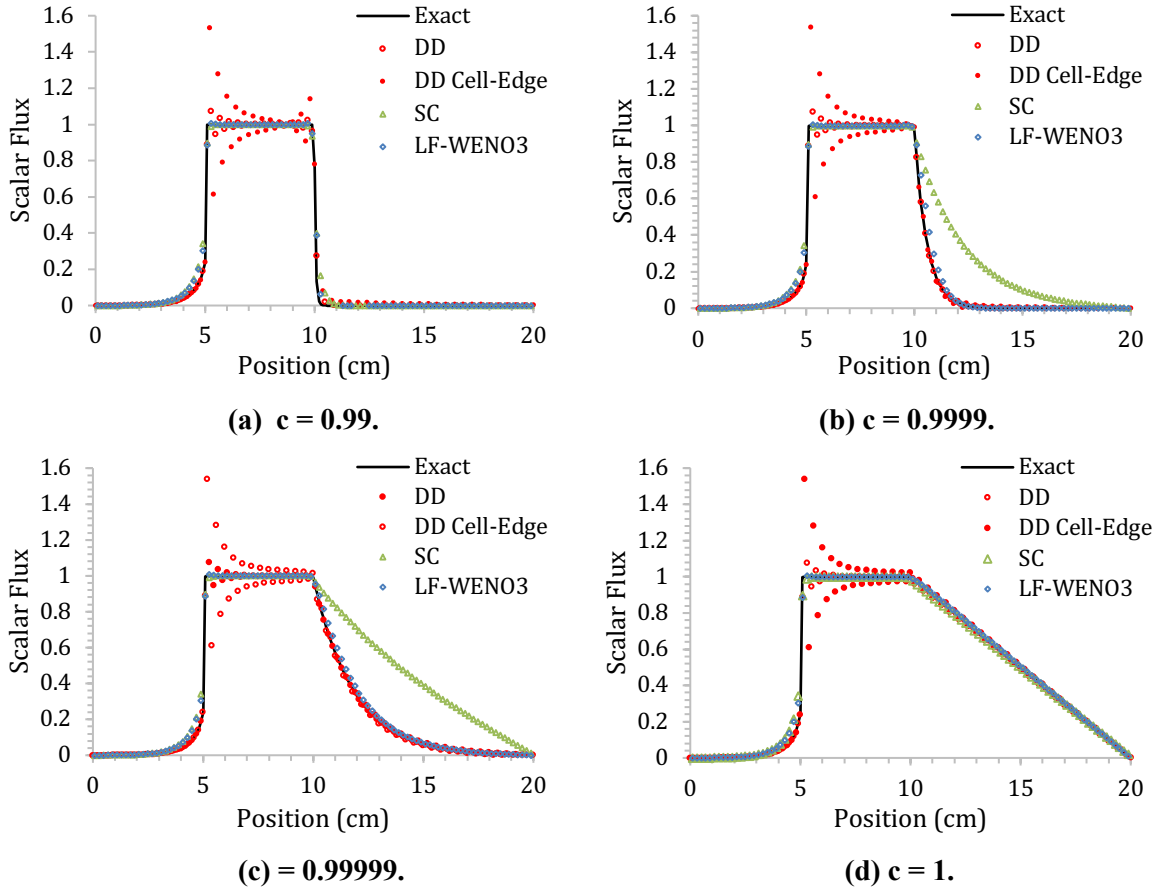
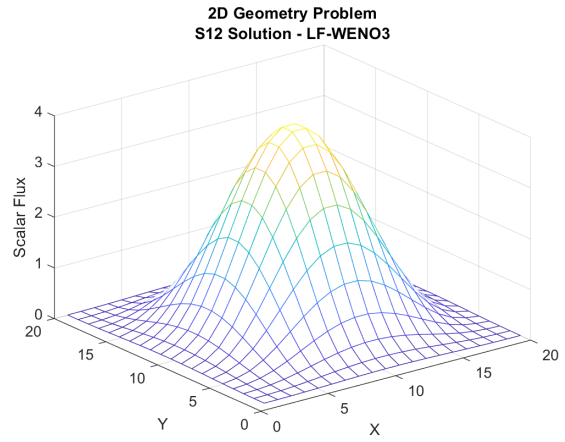
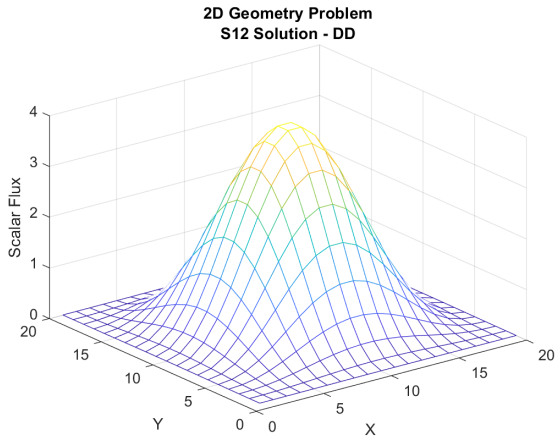


**Figure 4. 1-D Inhomogeneous Problem.**

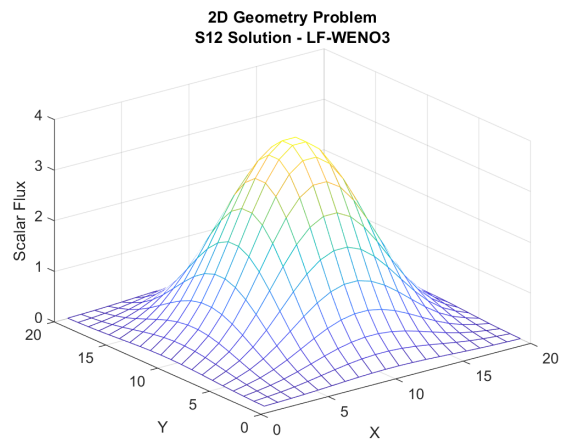
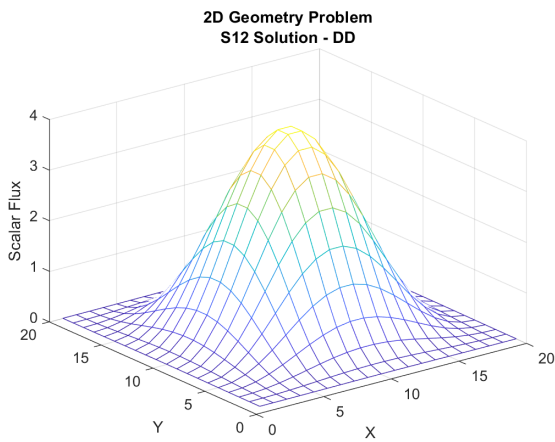
The third problem is a 2-D square problem with the vacuum boundary on each side. The angular flux is defined by the manufactured solution of Eq. (17). The numerical solutions are obtained using the level-symmetric  $S_{12}$  quadrature set for angular discretization. The cell-average source for the numerical solution is obtained by averaging  $Q(x, y)$  on each computational cell. The problem specifications are given as follows:

$$\begin{aligned} L \times L &= 2 \times 2, & h_x &= h_y = 0.1, \\ \Sigma_t &= 1000, & \Sigma_s &= 999; 999.9; 999.99, \end{aligned}$$

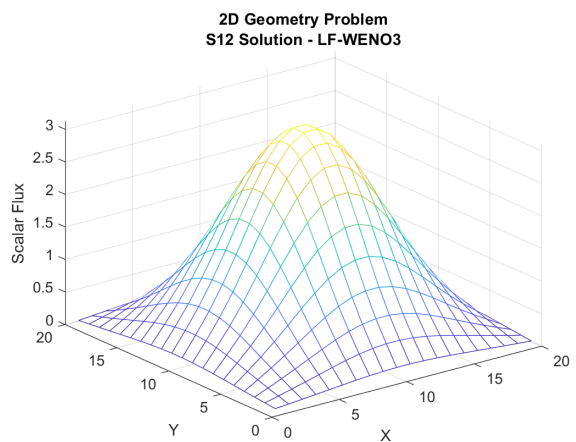
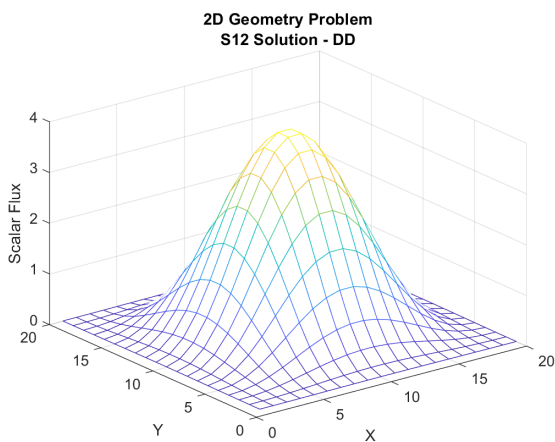
The problem is a very thick and diffusive problem with the cell optical thickness of 100 MFPS and the scattering ratio of 0.999–0.99999. The DD and LF-WENO3 calculated scalar fluxes for three scattering ratios are shown in Figure 5.



(a)  $c = 0.999$ .



(b)  $c = 0.9999$ .



(c)  $c = 0.99999$ .

**Figure 5. 2-D Problem ( $x$  and  $y$  denote cell number index).**

From the above numerical results, we have the following observations:

- a) As the optical thickness of the computational cells tends to infinite, the SC scheme becomes the first-order step upwind method, which is stable but has excessive numerical diffusion. SC fails for thick diffusive problems [9].
- b) As reported in the previous research [10], DD possesses the thick diffusion limit for isotropic incident boundary fluxes for 1-D and 2-D problems as shown in Figures 3 and 5. However, Figure 4 shows that DD solutions (both cell-average and cell-edge fluxes) become corrupted by unphysically oscillations in the presence of anisotropic boundary fluxes (where the boundary layer could develop). This is a typical issue for central difference based schemes due to lack of numerical diffusion.
- c) In general, LF-WENO3 does not possess the thick diffusion limit. Figure 3 shows that the accuracy of LF-WENO3 deteriorates as the problem becomes increasingly thick and diffusive. However, we can improve the accuracy by using a fine mesh with respect to the diffusion length ( $1/\sqrt{3\Sigma_t\Sigma_a}$ ) of the problem. For example, Figure 3d shows that the accuracy can be improved significantly when the finer mesh ( $h = 0.05\text{cm}$ ) is used for the case of  $\varepsilon = 0.001$ . The MFP of this case is only  $0.001\text{cm}$ , but the diffusion length is about  $0.65\text{cm}$ . Therefore, LF-WENO3 can attain very high accuracy on a very coarse mesh compared to MFP for thick diffusive problems as long as the mesh is fine enough in terms of the diffusion length. In addition, it should be noted that LF-WENO3 can use a relatively coarse mesh in terms of the diffusion length without loss of accuracy if the problem is thick but not too diffusive (e.g.,  $c > 0.99$ ). Numerical results show that LF-WENO3 approximately achieves the diffusion limit on the mesh size,  $\varepsilon^l h$ , where  $l = 1/3$ , i.e., between the thick ( $l = 0$ ) and intermediate ( $l = 1$ ) diffusion regimes [9]. A asymptotic analysis will be carried out to verify this observation in the future.
- d) The third problem is an interesting case, in which the flux is the fixed manufactured solution. When varying the scattering ratio, the source term has to be changed accordingly to maintain the same manufactured flux. The numerical solution of LF-WENO3 becomes worse as the scattering ratio increases (i.e., the problem becomes increasingly diffusive), although the diffusion length becomes relatively larger than the fixed mesh size. The diffusion length is  $0.0183\text{cm}$  for the case “ $c = 0.999$ ”, and  $0.183\text{cm}$  for the case “ $c = 0.99999$ ”. It is found that the accuracy can be improved significantly when using a finer mesh for the case “ $c = 0.9999$ ”. However, the deterioration does not happen with DD for this case, which indicates that DD possesses the thick diffusion limit, although the source is significantly non-uniform and non-isotropic. Further research is needed to study the property of LF-WENO3 for problems with a nonuniform and anisotropic source.
- e) In addition, Figure 4 shows that LF-WENO3 is much more stable than DD for inhomogeneous problems because LF-WENO3 has superior positivity preserving as demonstrated in [1].

#### 4. CONCLUSIONS

In this paper, we have presented the study of the spatial convergence rate of LF-WENO3 for the  $S_N$  solution based on the manufactured solution. It has been confirmed that LF-WENO3 can achieve the third-order spatial accuracy for sufficiently smooth problems. The performance of LF-WENO3 for thick diffusive problems has been demonstrated based on the three model problems. In general, LF-WENO3 does not have the thick diffusion limit. However, our numerical results have indicated that LF-WENO3 can attain the diffusion limit on a mesh of  $\varepsilon^{1/3}h$ , which is much coarser than the mesh for the intermediate regime ( $\varepsilon h$ ), whereas slightly finer than that for the thick diffusion regime ( $h$ ). An asymptotic analysis will be carried out to verify this observation in the future. Nevertheless, LF-WENO3 is a highly accurate and robust scheme

which can be applied to thick diffusive problems if the mesh size is sufficiently fine in terms of the diffusion length or the problem is not extremely diffusive.

## ACKNOWLEDGMENTS

This work was supported in part by the US Department of Energy Nuclear Energy University Program (NEUP).

## REFERENCES

1. D. Wang and T. Byambaakhuu, "High Order Lax-Friedrichs WENO Fast Sweeping Methods for the  $S_N$  Neutron Transport Equation," *Nucl. Sci. Eng.* (in press). <https://doi.org/10.1080/00295639.2019.1582316>.
2. C.Y. Kao, S. Osher and J. Qian, "Lax-Friedrichs sweeping schemes for static Hamilton-Jacobi equations," *J. Comput. Phys.*, **196**, 367–391 (2004).
3. W. Chen, C.-S. Chou, C.-Y. Kao, "Lax-Friedrichs fast sweeping methods for steady state problems for hyperbolic conservation laws," *J. Comput. Phys.* **234**, 452–471 (2013).
4. E. W. Larsen and J. B. Keller, "Asymptotic Solution of Neutron Transport Problems for Small Mean Free Paths," *J. Math. Phys.* **15**, 75 (1974).
5. G. J. Habetler and B. J. Matkowsky, "Uniform Asymptotic Expansion in Transport Theory with Small Mean Free Paths, and the Diffusion Approximation," *J. Math. Phys.* **16**, 846 (1974).
6. G. C. Papanicolaou, "Asymptotic Analysis of Transport Processes," *Bull. Am. Math. Soc.* **81**, 330 (1975).
7. E. W. Larsen, "Diffusion Theory as an Asymptotic Limit of Transport Theory for Nearly Critical Systems with Small Mean Free Paths," *Ann. Nucl. Energy* **7**, 249 (1980).
8. E. W. Larsen, G. C. Pomraning, and V. C. Badham, "Asymptotic Analysis of Radiative Transfer Problems," *J. Quant. Spectros. Radiat. Transfer* **29**, 285 (1983).
9. E. W. Larsen, J. E. Morel, and W. F. Miller, Jr., "Asymptotic Solutions of Numerical Transport Problems in Optically Thick, Diffusive Regimes," *J. Comput. Phys.* **69**, 283 (1987).
10. E. W. Larsen, J. E. Morel, "Asymptotic Solutions of Numerical Transport Problems in Optically Thick, Diffusive Regimes II," *J. Comput. Phys.* **83**, 212 (1989).
11. E. W. Larsen, "The Asymptotic Diffusion Limit of Discretized Transport Problems," *Nucl. Sci. Eng.* **112**, 336 (1992).
12. M. L. Adams, "Discontinuous Finite Element Transport Solutions in Thick Diffusive Problems," *Nucl. Sci. Eng.* **137**, 298 (2001).
13. J-C Guermond and G. Kanschat, "Asymptotic Analysis of Upwind Discontinuous Galerkin Approximation of the Radiative Transport Equation in the Diffusive Limit," *Siam. J. Numer. Anal.* **48**, 53 (2010).